Effect of Ni on the Formation and Growth of Primary Cu6Sn5 Intermetallics in Sn-0.7 wt.%Cu Solder Pastes on Cu Substrates During the Soldering Process

M.A.A. Mohd Salleh,[1,2,5,6] S.D. Mcdonald,[1] C.M. Gourlay,[3] S.A. Belyakov,[3] H. Yasuda,[4] And K. Nogita[1]

1.—Nihon Superior Centre for the Manufacture of Electronic Materials (NS CMEM), School of Mechanical and Mining Engineering, The University of Queensland, St Lucia, QLD 4072, Australia.

2.—Centre of Excellence Geopolymer and Green Technology, School of Materials Engineering, Universiti Malaysia Perlis (UniMAP), Taman Muhibbah, 02600 Jejawi, Arau, Perlis, Malaysia.

3.—Department of Materials, Imperial College, London SW7 2AZ, UK.

4.—Department of Materials Science and Engineering, Kyoto University, Sakyo-ku, Kyoto 606-8501, Japan.

5.—e-mail: m.mohdsalleh@uq.edu.au

6.—e-mail: arifanuar@unimap. edu.my

ABSTRACT

This paper investigates the effect of 0.05 wt.% Ni on the formation and growth of primary Cu_6Sn_5 in Sn-0.7 wt.%Cu solder paste soldered on a Cu substrate, using a real-time synchrotron imaging technique. It was found that small additions of Ni significantly alter the formation and growth of the primary Cu_6Sn_5 intermetallics, making them small. In contrast, without Ni, primary Cu_6Sn_5 intermetallics tend to continue growth throughout solidification and end up much larger and coarser. The primary effect of the Ni addition appears to be in promoting the nucleation of a larger amount of small Cu_6Sn_5. The results provide direct evidence of the sequence of events in the reaction of Nicontaining Sn-0.7 wt.%Cu solder paste with a Cu substrate, and in particular the formation and growth of the primary Cu_6Sn_5 intermetallic

INTRODUCTION

Electric and electronic devices have rapidly become more advance and denser necessitating stronger and higher reliability interconnects and advances in solder materials. Among commercially available lead-free solders, Sn-0.7wt%Cu solder systems were widely used in wave soldering due to their availability and low cost [1, 2]. However, Sn-0.7wt%Cu has poor mechanical properties and is prone to brittle whisker intermetallic compound (IMC) growth and formation of large primary η-Cu_6Sn_5 in the solder matrix and a thick interfacial IMC layer consisting of η-Cu_6Sn_5 and ε-Cu_3Sn, that can lead to serious reliability concerns [3]. Due to this disadvantage, many researches has been undertaken on the micro-alloying effects of several elements in the Sn-Cu solder system including Ni [4-8], Zn [6], Bi [9], In [10] and Al [11, 12]. These micro-alloying attempts have been made to improve the mechanical properties of a solder joint. Within the range of alloys developed, the near eutectic composition of Sn-0.7wt%Cu with Ni trace level elemental additions has found application in wave soldering processes [13, 14]. Zeng et al. [6] had reported that with concurrent additions of Ni and Zn there is a significant refinement of the microstructure and a more stable interfacial Cu_6Sn_5 intermetallic is obtained. In addition, Yoon et al. [15] had investigated the growth of interfacial Cu_6Sn_5 in Sn-Cu-Ni solders after thermal ageing and identified that the interfacial intermetallic compound (IMC) activation energy was considered low compared to the activation energy of interfacial IMC in binary Sn-Cu solders. In another study, Yang et al. [7] had reported that with Ni additions to Sn-0.7wt%Cu the growth of Cu_3Sn interfacial IMC was suppressed which also resulted in the formation of fine needle-like $(Cu,Ni)_6Sn_5$ at the solder/substrate interface. In addition, the reported effects of small additions of Ni in Sn-0.7wt%Cu solder alloys have included better fluidity [14, 16], alterations to the eutectic composition and promotion of a near eutectic Sn-Cu_6Sn_5 microstructure, stabilisation of the hexagonal high temperature phase of Cu_6Sn_5 [17], and suppression of cracking in Cu_6Sn_5 solder joints formed between Sn-0.7wt%Cu solders and Cu substrates [18]. However, most of these investigations on IMC formation in Sn-Cu and Sn-Cu-Ni solder systems were ex-situ experiments and focused on the interfacial IMC rather than the primary IMC that forms in the solder matrix.

In an attempt to investigate the growth of IMCs, recent in-situ real time imaging has been conducted by Wang et al. [19], Qu et al. [20, 21] and Huang et al. [22]. Recently we have successfully developed [23] a synchrotron based in-situ method to observe, in real time, the entire soldering process of a solder paste on a Cu substrate, including the solid-liquid-solid transition to provide an understanding on the real-time primary intermetallic growth. In this study, we use this technique to observe the soldering of Sn-0.7wt%Cu and Sn-0.7wt%Cu-

0.05wt%Ni solder paste on a Cu substrate in order to investigate the influence of Ni addition on the formation and growth of the primary Cu_6Sn_5 intermetallic.

EXPERIMENTAL PROCEDURE

The real time observation experiments were performed at BL20XU beamline in the SPring-8 synchrotron using an in-situ synchrotron X-ray real time solidification observation setup developed in previous research [23-25]. The parameters were chosen to allow a high degree of coherence, absorption contrast and phase contrast enabling boundaries in the sample to be observed on transmitted images. These image signals collected are then converted into a digital format of 2000 X 2000 pixels at 1 mm X 1 mm giving a resolution of 0.477 µm per pixel. A planar undulator was used as a light source and the radiation was monochromatized with Si double crystal monochromators. An exposure time of 1s per frame to capture the images was used. To mimic the process of reflow soldering, a furnace with graphite heating elements where heat is transferred through radiation in an enclosed sample chamber was used (Figure 1a). The sample position and sample cell configuration is shown in Figure 1b, and each sample of either Sn-0.7wt%Cu or Sn-0.7wt%Cu-0.05wt%Ni solder paste supplied by Nihon Superior Co Ltd had an average solder spheres sizes of 35 µm and was placed vertically on a thin 100 µm Cu substrate. The observation window area of 10 x 10 mm^2 with a vent for flux outgassing was made by using a 100 µm thickness poly-tetrafluoroethylene (PTFE) sheet placed between two SiO_2 plates. Samples were set to be heated from room temperature to approximately 250^0C at 0.33^0C/s and held for 30 s before cooling down at approximately 0.33^0C/s. The soldering temperature profiles for the experiments are shown in Figure 1c.

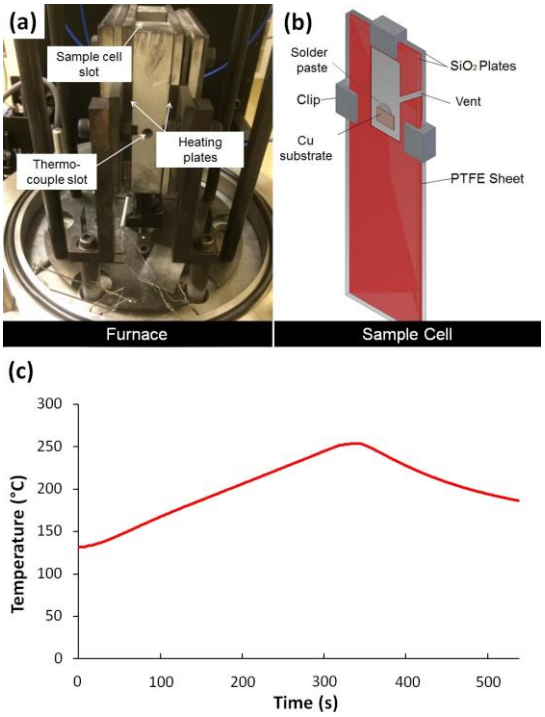

Figure 1: (a) Synchrotron real-time in-situ observation heating furnace setup, (b) soldering sample cell setup, and (c) example temperature profile.

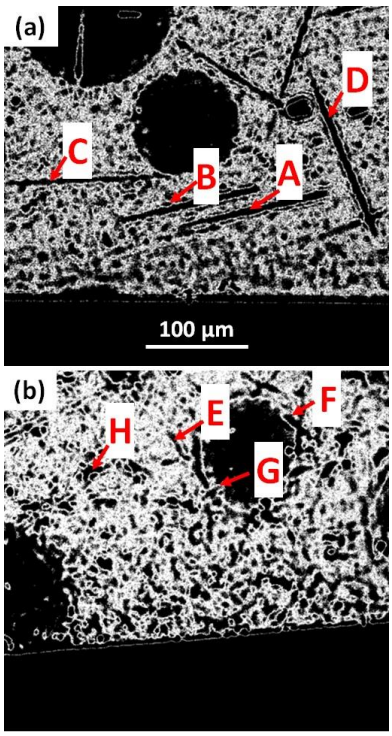

Figure 2: Threshold image of X-ray synchrotron images using ImageJ software for measuring primary intermetallic compound (IMC) of (a) Cu_6Sn_5 on Sn-0.7wt%Cu and (b) $(Cu,Ni)_6Sn_5$ on Sn-0.7wt%Cu-

0.05wt%Ni. Individual primary Cu_6Sn_5 particles are labeled with letters corresponding to the particles shown in Figure 3(i) and Figure 4(i).

The size of primary intermetallics on Sn-0.7wt%Cu and Sn-0.7wt%Cu-0.05wt%Ni solder pastes on Cu substrates was measured using ImageJ software, a freeware Java based image processing program. Synchrotron radiography images were then processed by using a threshold method [26] to obtain an accurate measurement. Several primary intermetallic of each solder alloy were chosen for measurement as indicated in Figure 2. Post synchrotron in-situ observation, samples were polished and scanning electron microscopy (SEM) images were obtained using backscattered mode. Electron dispersive X-ray spectroscopy (EDS) mapping was conducted to observe the Ni and Cu distribution.

RESULTS AND DISCUSSION

Figure 3 reveals the real-time observations of reactions between Sn-0.7wt%Cu solder paste and the Cu substrate at experimental time of (a) 292 s, (b) 305 s, (c) 306 s, (d) 423 s, (e) 430 s, (f) 436 s, (g) 444 s, (h) 450 s and (i) 458 s. From the observations, Sn-0.7wt%Cu solder paste which contains solder spheres and flux starts to transform to a more viscous suspension (Figure 3a) at approximately 241°C and eventually the solder spheres contained in the suspension tend to fully melt after a few seconds as seen in Figure 3b. The liquid Sn-0.7wt%Cu then immediately tends to wet the Cu substrate followed by near instantaneous formation of interfacial Cu_6Sn_5 IMC. From Figure 3c, it can be seen that at the moment the molten solder contacts the solid Cu an instant planar (within the resolution of the imaging) intermetallic layer of significant thickness forms, while molten solder flows onto the Cu substrate. After a peak temperature of 250°C for 30 s, the solder then was cooled down. During cooling (Figure 3d-3i), primary rod-shaped Cu_6Sn_5 intermetallics nucleated at 425 – 430 s of the experimental time at approximately 218 – 212°C. The large primary rod-shaped Cu_6Sn_5 tend to grow during cooling before solidification is complete.

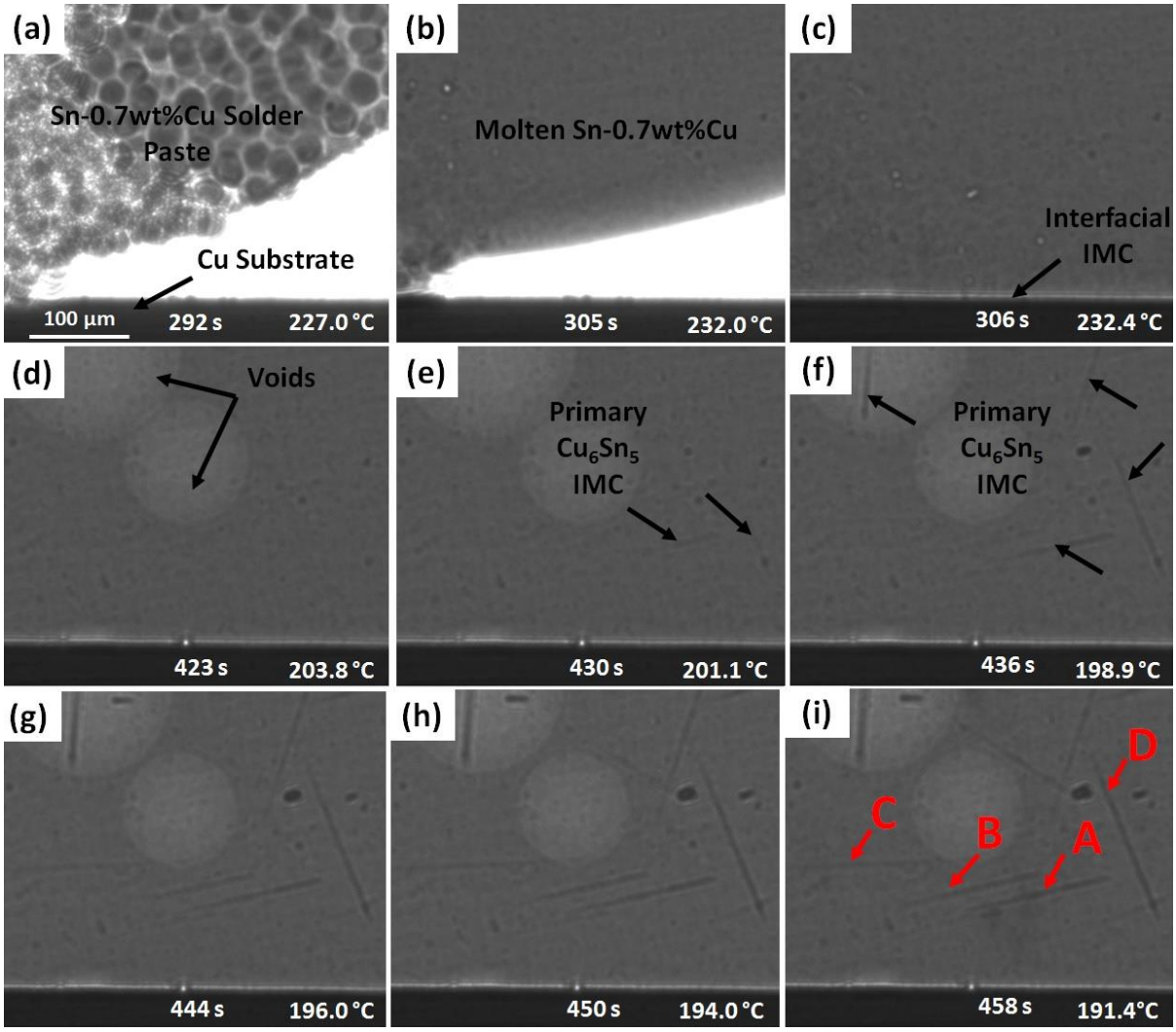

Figure 3: Real-time observations of reactions between Sn-0.7wt%Cu solder paste and the Cu substrate at experimental time of (a) 292 s, (b) 305 s, (c) 306 s, (d) 423 s, (e) 430 s, (f) 436 s, (g) 444 s, (h) 450 s and (i) 458 s.

Figure 4 reveals the real-time observation of the reaction between Sn-0.7wt%Cu-0.05wt%Ni solder paste and the Cu substrate at an experimental time of (a) 197 s, (b) 202 s, (c) 223 s, (d) 330 s, (e) 335 s, (f) 339 s, (g) 350 s, (h) 360 s and (i) 367 s. From the observations, similar to the Sn-0.7wt%Cu solder paste which contains solder spheres and flux starts to transform to a more viscous suspension (Figure 4a) at approximately 236°C and the solder spheres contained in suspension tend to fully melt after a few seconds. The liquid Sn-0.7wt%Cu-0.05wt%Ni then immediately wets the Cu substrate and interfacial Cu_6Sn_5 IMC formation occurs (Figure 4c). During cooling (Figure 4d-4i), small flake-like primary Cu_6Sn_5 intermetallics nucleate and grow to a scale of a few tens of µm in length at 330 – 340 s of the experimental time at approximately 234 – 231°C. Similar to the

large primary Cu_6Sn_5 intermetallic in the Ni free Sn-0.7wt%Cu, the small primary flake-like Cu_6Sn_5 intermetallics tends to nucleate and grow with increasing time during cooling before solidification. Due to the density difference with the liquid, these small flake-like Cu_6Sn_5 intermetallics tend to settle down at the interface between the molten solder and Cu substrate. However it is clear that these particles do not form at the substrate but in the bulk of the solder.

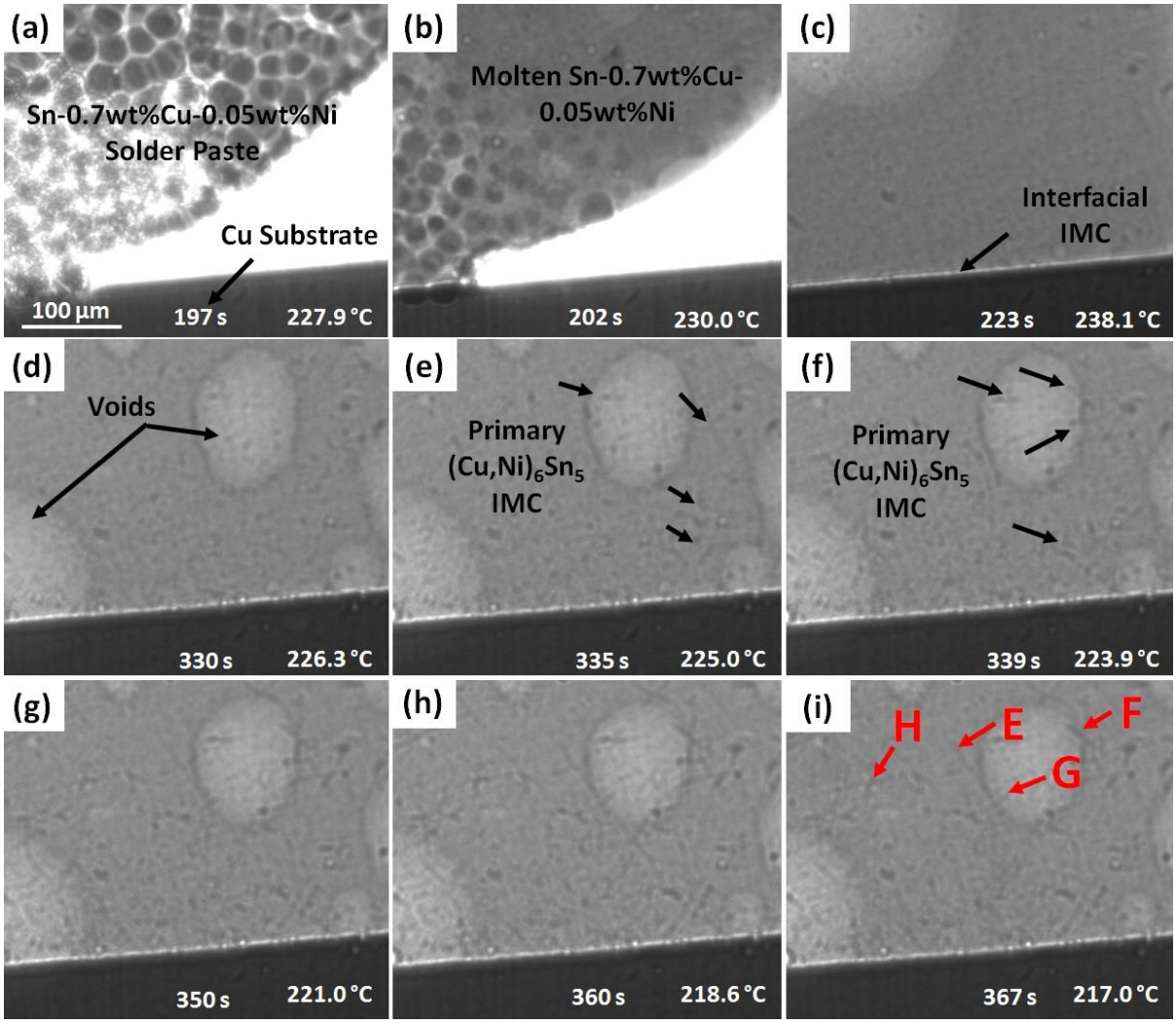

Figure 4: Real-time observations of reactions between Sn-0.7wt%Cu-0.05wt%Ni solder paste and the Cu substrate at experimental time of (a) 197 s, (b) 202 s, (c) 223 s, (d) 330 s, (e) 335 s, (f) 339 s, (g) 350 s, (h) 360 s and (i) 367 s.

In both samples at early stages of molten solder reacting with the Cu substrate, the liquid solder results in the rapid dissolution of Cu from the Cu substrate which then forms a near instantaneous planar interfacial IMC. The formation of Ƞ-Cu_6Sn_5 interfacial IMC becomes possible after the Cu substrate/liquid solder interface becomes

supersaturated and since both Sn-0.7wt%Cu and Sn-0.7wt%Cu-0.05wt%Ni are near eutectic alloys, the planar η-Cu_6Sn_5 forms rapidly (i.e. it does not take much excess copper to put these alloys into the primary Cu_6Sn_5 phase field). Subsequently after the formation of the interfacial IMC layer, the Cu concentration at the liquid solder matrix progress through a transient stage. In the Sn-0.7wt%Cu-0.05wt%Ni solder alloys, the interfacial IMCs are known to be finer needle-like shaped η-Cu_6Sn_5 [7] with a larger grain boundary area and provide a large area of molten solder in contact with the initial interfacial IMC. In comparison with Sn-0.7wt%Cu solder, scallop shaped η-Cu_6Sn_5 interfacial IMCs are known to form [7] with a smaller grain boundary area in contact with molten solder. With a larger grain boundary area in contact with the molten solder, Cu atoms diffuse faster. As a result, the Cu concentration from the solder matrix and a faster Cu atom diffusion from the Cu substrate occurs allowing the primary Cu_6Sn_5 intermetallic at the solder matrix of Sn-0.7wt%Cu-0.05wt%Ni alloy to form earlier during cooling at approximately 234 – 231°C compared to the Sn-0.7wt%Cu solder alloy at 218 – 212°C. In addition, in both solder alloys, due to the large undercooling of Sn, the primary Cu_6Sn_5 forms before the Sn dendrites nucleate. Sn dendrites had formed and grow rapidly which were hard to be captured in this experiment (with an exposure time of 1s per frame) due to the rapid growth during solidification.

For the primary Cu_6Sn_5 growth investigations of both solder alloys, four individual intermetallic Cu_6Sn_5 particles were chosen and measured which are indicated as A, B, C, and D for Sn-0.7wt%Cu and E, F, G and H for Sn-0.7wt%Cu-0.05wt%Ni (Figure 2, Figure 3i and Figure 4i). In Figure 5, the evolution of primary Cu_6Sn_5 intermetallics in Sn-0.7wt%Cu and Sn-0.7wt%Cu-0.05wt%Ni during cooling are plotted. It is obviously that the sizes of primary Cu_6Sn_5 intermetallics in Sn-0.7wt%Cu-0.05wt%Ni are smaller compared to Sn-0.7wt%Cu with approximately 150 – 350 μm^2 and 1300 – 1800 μm^2 in area size, respectively. As in Figure 5a, the primary Cu_6Sn_5 intermetallic in Sn-0.7wt%Cu tends to continue to grow until the molten solder solidifies while in Sn-0.7wt%Cu-0.05wt%Ni, the growth is restricted before solidification appears to be complete. From the graph, the growth of the primary intermetallics was faster in the Sn-0.7wt%Cu-0.05wt%Ni. In addition, from Figure 4, it is clearly observed that Sn-0.7wt%Cu-0.05wt%Ni promotes nucleation of a larger amount of small flake-like Cu_6Sn_5. A range of factors could be responsible for the smaller and more numerous primary Cu_6Sn_5 in Sn-0.7wt%Cu-0.05wt%Ni/Cu than in Sn-0.7wt%Cu/Cu. For example, (i) it is feasible that Ni introduces nucleation sites to the melt, and (ii) Ni could alter the thermodynamics and affect the solid fraction versus temperature curve and/or the constitutional supercooling that develops ahead of the Cu_6Sn_5 crystals. Indeed, dilute Ni additions have been shown to significantly alter the shape of the Cu_6Sn_5 liquidus line/surface [27].

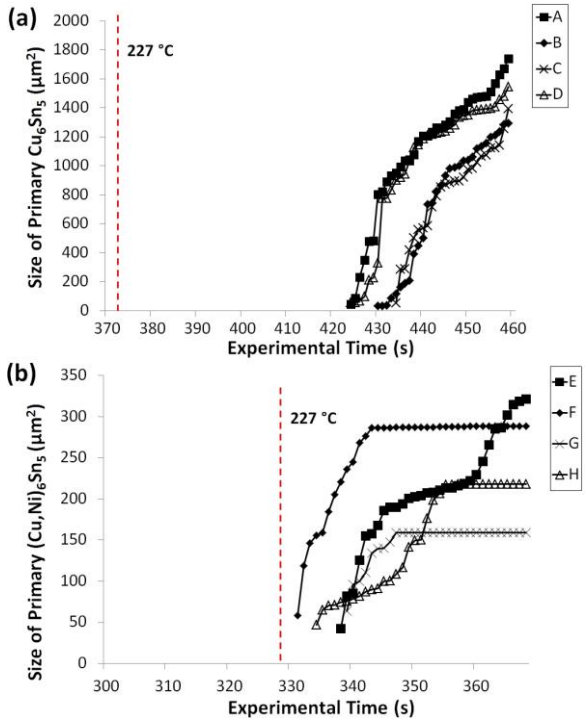

Figure 5: Evolution of primary Cu_6Sn_5 intermetallic growth of (a) Sn-0.7wt%Cu and (b) Sn-0.7wt%Cu-0.05wt%Ni, during cooling.

Subsequent to the in-situ observation, samples were taken out from the experiment sample cell and prepared for further metallographic observations including SEM coupled with electron dispersive x-ray spectroscopy (EDS) for further SEM imaging and element mapping to observe the Ni and Cu distribution relative to the interfacial and primary intermetallics. Figure 6 shows the Sn L and Cu K maps on which it is clearly observed that the Cu K distributions are associated primarily with the large rod-shape primary Cu_6Sn_5 and at the interfacial IMC layer of Sn-0.7wt%Cu. On the other hand, Figure 7 shows the distribution of Sn L, Ni K and Cu K of Sn-0.7wt%Cu-0.05wt%Ni which implies a difference between the Cu behavior in the Ni free alloy and the Ni location in the Ni containing alloy.

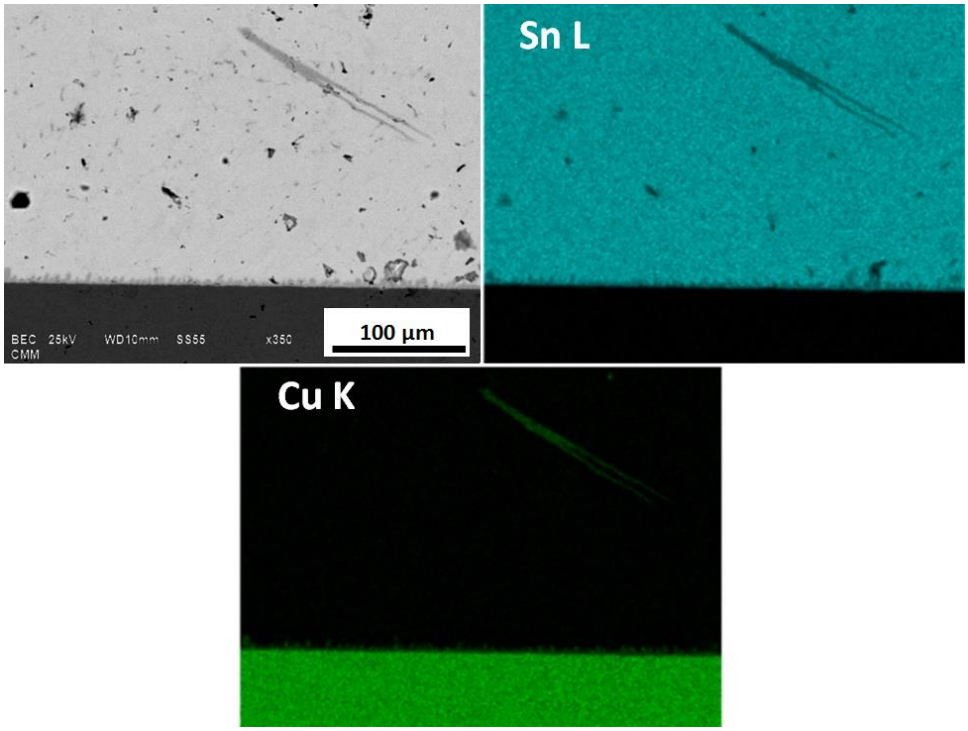

Figure 6: Backscattered SEM image and EDS mapping images of Sn-0.7wt%Cu taken subsequent to the synchrotron experiments.

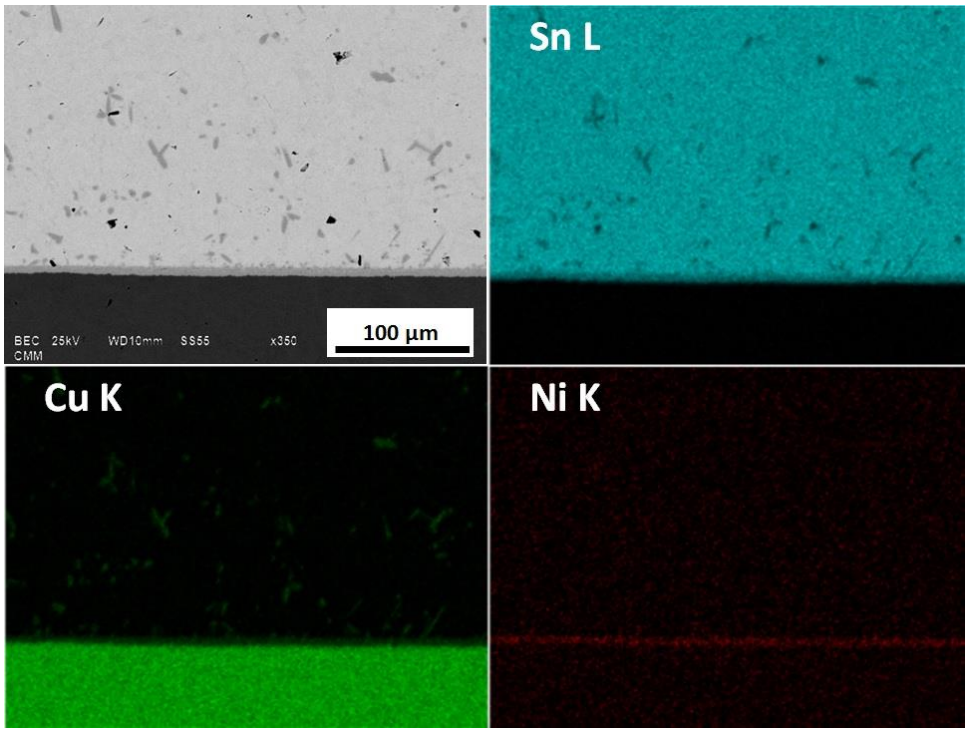

Figure 7: Backscattered SEM image and EDS mapping images of Sn-0.7wt%Cu-0.05wt%Ni taken subsequent to the synchrotron experiments.

CONCLUSIONS

The entire soldering process of solder pastes on Cu substrates was successfully observed using a real-time synchrotron imaging technique to investigate the formation and growth of primary Cu_6Sn_5 intermetallic in the solder matrix of Sn-0.7wt%Cu and Sn-0.7wt%Cu-0.05wt%Ni solder pastes during soldering. With 0.05wt% of Ni addition to Sn-0.7wt%Cu, the nucleation and growth of the primary Cu_6Sn_5 intermetallic was significantly altered. The morphologies of primary Cu_6Sn_5 intermetallic are observed to be large and rod shaped in Sn-0.7wt%Cu solder paste while small flake-like Cu_6Sn_5 particles were observed in Sn-0.7wt%Cu-0.05wt%Ni solder paste.

ACKNOWLEDGEMENTS

The authors gratefully acknowledge financial support from the University of Queensland (UQ)-Nihon Superior (NS) collaboration research programme. The authors thank Dr. K. Uesugi and Dr. A. Takeuchi of SPring-8 beamline scientist, Professor Akira Sugiyama from the Osaka Sangyo University, Dr. T. Nagira from Osaka University and students from the Department of Materials Science and Engineering, Kyoto University. The authors would also like to thank Dr. Christopher Gourlay from Imperial College London for valuable discussions. Real-time observation experiments were performed at the SPring-8 BL20XU (Project ID: 2014B1620 and 2015A1675). We acknowledge travel funding provided by the Australian Synchrotron International Synchrotron Access Program (AS/IA143/9218 and AS/IA151/9538) managed by the Australian Synchrotron and funded by the Australian government. SEM imaging and EDS mapping were performed at the Centre for Microscopy and Microanlaysis (CMM), the University of Queensland. Mohd Salleh is financially supported by the Malaysian Education Ministry and University Malaysia Perlis (UniMAP).

REFERENCES

[1] X. Li, F. Zhang, F. Zu, X. Lv, Z. Zhao, D. Yang, Journal of Alloys and Compounds, 505 (2010) 472-475.

[2] H. Wang, F. Wang, F. Gao, X. Ma, Y. Qian, Journal of Alloys and Compounds, 433 (2007) 302-305.

[3] P.E. Gary Delserro, in: Delserro Engineering Solutions, EE Evaluation Engineering, Easton, PA 2006.

[4] A.E. Hammad, Materials & Design, 50 (2013) 108-116.

[5] F. Cheng, H. Nishikawa, T. Takemoto, J Mater Sci, 43 (2008) 3643-3648.

[6] G. Zeng, S.D. McDonald, Q. Gu, Y. Terada, K. Uesugi, H. Yasuda, K. Nogita, Acta Materialia, 83 (2015) 357-371.

[7] C. Yang, F. Song, S.W. Ricky Lee, Microelectronics Reliability, 54 (2014) 435-446.

[8] B.L. Silva, N. Cheung, A. Garcia, J.E. Spinelli, Journal of Alloys and Compounds, 632 (2015) 274-285.

[9] X. Hu, K. Li, Z. Min, Journal of Alloys and Compounds, 566 (2013) 239-245.

[10] M. Kamal, T. El-Ashram, Materials Science and Engineering: A, 456 (2007) 1-4.

[11] S. McDonald, K. Nogita, J. Read, T. Ventura, T. Nishimura, Journal of Elec Materi, 42 (2013) 256-262.

[12] J.W. Xian, S.A. Belyakov, T.B. Britton, C.M. Gourlay, Journal of Alloys and Compounds, 619 (2015) 345-355.

[13] C.M. Gourlay, K. Nogita, A.K. Dahle, Y. Yamamoto, K. Uesugi, T. Nagira, M. Yoshiya, H. Yasuda, Acta Materialia, 59 (2011) 4043-4054.

[14] T. Ventura, C. Gourlay, K. Nogita, T. Nishimura, M. Rappaz, A. Dahle, Journal of Electronic Materials, 37 (2008) 32-39.

[15] J.-W. Yoon, Y.-H. Lee, D.-G. Kim, H.-B. Kang, S.-J. Suh, C.-W. Yang, C.-B. Lee, J.-M. Jung, C.-S. Yoo, S.-B. Jung, Journal of Alloys and Compounds, 381 (2004) 151-157.

[16] T. Ventura, K. Nogita, C.M. Gourlay, T. Nishimura, M. Rappaz, A.K. Dahle, in: 5th Decennial International Conference on Solidification Processing, Sheffield, UK, 2007, pp. 651-655.

[17] K. Nogita, Intermetallics, 18 (2010) 145-149.

[18] K. Nogita, C.M. Gourlay, T. Nishimura, JOM, 61 (2009) 45-51.

[19] T. Wang, P. Zhou, F. Cao, H. Kang, Z. Chen, Y. Fu, T. Xiao, W. Huang, Q. Yuan, Intermetallics, 58 (2015) 84-90.

[20] L. Qu, H.T. Ma, H.J. Zhao, A. Kunwar, N. Zhao, Applied Surface Science, 305 (2014) 133-138.

[21] L. Qu, N. Zhao, H.J. Zhao, M.L. Huang, H.T. Ma, Scripta Materialia, 72–73 (2014) 43-46.

[22] M.L. Huang, Z.J. Zhang, N. Zhao, Q. Zhou, Scripta Materialia, 68 (2013) 853-856.

[23] M.A.A.M. Salleh, S.D. McDonald, H. Yasuda, A. Sugiyama, K. Nogita, SCRIPTA MATER, 100 (2015) 17-20.

[24] H. Yasuda, I. Ohnaka, K. Kawasaki, A. Sugiyama, T. Ohmichi, J. Iwane, K. Umetani, Journal of Crystal Growth, 262 (2004) 645-652.

[25] K. Nogita, H. Yasuda, A. Prasad, S.D. McDonald, T. Nagira, N. Nakatsuka, K. Uesugi, D.H. StJohn, Materials Characterization, 85 (2013) 134-140.

[26] R. Tajima, Y. Kato, Field Crops Research, 121 (2011) 460-463.

[27] C.M. Gourlay, K. Nogita, J. Read, A.K. Dahle, Journal of Elec Materi, 39 (2010) 56-69.